Journal of
Experimental and Theoretical Analyses

MDPI

Article

Advancing Pressure-Based Flow Rate Soft Sensors: Signal Filtering Effects and Non-Laminar Flow Rate Determination

Faras Brumand-Poor *, Tim Kotte, Abdulaziz Hanifa, Christian Reese, Marius Hofmeister and Katharina Schmitz

Institute for Fluid Power Drives and Systems (ifas), RWTH Aachen University, 52074 Aachen, Germany
* Correspondence: faras.brumand@ifas.rwth-aachen.de; Tel.: +49-241-80-47743

Abstract: Precise flow measurement is crucial in fluid power systems. Especially in combination with pressure, hydraulic power can be particularly beneficial for predictive maintenance and control applications. However, conventional flow sensors in fluid power systems are often invasive, thus disrupting the flow and yielding unreliable measurements, especially under transient conditions. A common alternative is to estimate the flow rate using pressure differentials along a pipe and the Hagen–Poiseuille law, which is limited to steady, laminar, and incompressible flows. This study advances a previously introduced analytical soft sensor, demonstrating its ability to accurately determine the transient pipe flow beyond laminar conditions, without requiring a dedicated flow rate sensor. This method provides a robust and computationally efficient solution for real-world hydraulic systems by applying two pressure transducers. A key contribution of this work is the investigation of signal filtering, revealing that even a simple first-order low-pass filter with a 100 Hz cutoff frequency significantly improves accuracy, which is demonstrated for pulsation frequencies of 5, 10, and 15 Hz, where the filtered results closely match experimental data from a test rig. These findings underscore the soft sensor's potential as a reliable alternative to traditional flow sensors, offering high accuracy with minimal computational overhead for a wide range of flow conditions.

Keywords: soft sensor; volumetric flow rate determination; non-laminar flow; signal filtering

Academic Editor: Marco Rossi

Received: 31 December 2024
Revised: 2 February 2025
Accepted: 25 February 2025
Published: 4 March 2025

Citation: Brumand-Poor, F.; Kotte, T.; Hanifa, A.; Reese, C.; Hofmeister, M.; Schmitz, K. Advancing Pressure-Based Flow Rate Soft Sensors: Signal Filtering Effects and Non-Laminar Flow Rate Determination. *J. Exp. Theor. Anal.* **2025**, *3*, 8. https://doi.org/10.3390/jeta3010008

1. Introduction

Measuring the volumetric flow guarantees hydraulic systems' optimal performance and longevity. Accurate flow rate data are essential for condition monitoring, predictive maintenance, and control engineering in both mobile and stationary hydraulic systems. When combined with pressure measurements, the flow rate enables the calculation of hydraulic power, which is a critical parameter for assessing system efficiency and identifying potential losses. Furthermore, volumetric flow represents a crucial control variable in fluid power systems.

The current range of volumetric flow sensors has two significant limitations. Many of these sensors are invasive, requiring installation within the pipe and often utilizing turbines or rotors that disrupt the flow and add mechanical complexity. Furthermore, these sensors frequently depend on inert components, which diminishes their efficacy at high frequencies. For instance, gauging pump pulsations is difficult, as the pulsation frequency depends on the pump's displacement units and rotational speed, often exceeding the range of conventional sensors. These limitations underscore the need for alternative solutions. The ideal sensor would be minimally invasive, capable of detecting transient

flow conditions, and functioning as a soft sensor by leveraging the pressure signals already present in hydraulic systems.

The concept of deriving flow rates from pressure signals has a long history. Analytical methods for calculating volumetric flow date back to the 19th century, with the Hagen–Poiseuille (HP) law being one of the most well-known. While this law is effective for steady, laminar flows, it does not account for transient or high-frequency effects. The Richardson effect is an example of a phenomenon affecting higher frequencies' velocity profiles [1]. By incorporating a dynamic term into the HP equation, it is possible to estimate transient flow rates. This study builds on these principles by introducing a soft sensor to compute transient flow rates based on pressure data.

In previously published work, an analytical soft sensor has been derived, which computes transient, compressible pipe flow based on pressure transducer signals [2,3]. This soft sensor has been validated by parameter-distributed simulations and a test rig [4,5]. The test rig was specifically constructed for this soft sensor and underlined its accuracy for real-world applications. The validation has been conducted for pipe flows inside the laminar regime and should now be extended to non-laminar flow. Furthermore, the importance of filtering the real-world pressure signals is one of the main scopes of this research.

This paper is structured as follows: Section 2.1 provides an overview of volumetric flow measurement techniques and models. Afterward, the basic structure for the analytical model is introduced in Section 2.2. Section 2.3 presents the test rig for the validation, and eventually, the investigated test cases are described in Section 2.4. In the following Section 3, the results are presented, and finally, the discussion and conclusions are provided in Sections 4 and 5.

2. Materials and Methods

2.1. Flow Rate Measurement Methods & Models

The accurate measurement of volumetric flow is a fundamental aspect of optimizing fluid systems' performance and is a key driver in developing a range of sensor technologies. These sensors are broadly classified into two categories as follows: invasive and non-invasive.

Invasive sensors, such as positive displacement and turbine flow meters, measure flow by tracking the movement of fluid volumes over time. However, the inertia of their components limits their ability to measure transient flows [6] accurately. A common invasive approach is to measure the pressure drop across a flow-restricting component, such as an orifice [7], using the following equation:

$$Q_O = \alpha_D A_D \sqrt{\frac{2\Delta p}{\rho}} \tag{1}$$

This relationship depends on parameters such as orifice geometry A_D, the discharge coefficient α_D, fluid density ρ, and pressure difference Δp. While viscosity has a minimal effect, obstructions disrupt flow patterns. Differential pressure meters, which rely on Bernoulli's principle, struggle with unsteady flows and become unreliable for frequencies above 2 Hz [8]. Other invasive methods, such as vortex flow meters and hot-wire anemometry, face challenges in low turbulence or provide localized measurements, often disturbing the flow.

Non-invasive sensors, including electromagnetic and ultrasonic flowmeters, do not disturb the flow. Electromagnetic flowmeters require conductive fluids, making them unsuitable for most hydraulic oils [7]. Ultrasonic flowmeters, while capable of transient flow measurement, assume symmetrical flow profiles, reducing accuracy in turbulent conditions [9].

Advanced minimally invasive techniques, such as particle image velocimetry and Coriolis flowmeters, offer innovative solutions but face practical limitations. Particle image velocimetry requires transparent tubes and seeding particles, while Coriolis flowmeters are constrained by tube resonance frequencies that limit response times [7,10].

Despite the advances in this field, most sensors are ill-suited for transient flows. They either lack the necessary response times or impose impractical requirements for industrial applications.

The recent advancements in transient flow measurement have resulted in the development of innovative methods and models that have enhanced the accuracy and reliability of the field. Brereton et al. introduced techniques for laminar pipe flow, relating flow rate to the history of pressure gradients without assuming velocity profiles [11]. Subsequently, an alternative approach was proposed, linking flow rate to centerline velocity history [12]. Sundstrom et al. enhanced friction modeling, thereby markedly reducing errors in the pressure-time method for hydraulic flow measurement [13]. Foucault et al. developed a real-time laminar flow estimation method based on differential pressure measurements and kinetic energy principles [14]. García et al. furthered the study of turbulent flow, developing models to simulate unsteady flow responses and laminarization phenomena [15,16].

In their comprehensive reviews of analytical models for accelerated incompressible fluid flow, Urbanowicz et al. addressed the challenges inherent in turbulent flow predictions [17]. Additionally, they developed analytical solutions for laminar water hammer phenomena and wall shear stress during water hammer events, which were validated by simulations and experiments [18].

Bayle et al. advanced the field of wave propagation models in viscoelastic pipes, creating a rheology-based model and a Laplace-domain approach applicable to diverse boundary conditions [19,20]. These developments span methods for transient flow estimation, improved friction and wave propagation modeling, and analytical solutions, enabling more accurate measurements for laminar and turbulent flows.

Hucko et al. [21] recently introduced a soft sensor-based method for measuring the volumetric flow rate by evaluating the forces acting on a valve. A significant advantage of this technique is that it requires only a minimal inlet size for proper flow development.

2.2. Pressure-Based Flow Rate Soft Sensor

An overview of the calculation steps within the soft sensor is given in Figure 1. The steps include setting the system parameters, such as the pipe's radius and length, and measuring the two input pressure signals. For the calculation, the soft sensor needs the derivative of the pressure signals. To take the derivative, the pressure signals must be filtered to handle the noise in the measurements. Afterward, the stationary and the dynamic flow rate can be calculated. Combining these two yields the final transient flow rate.

The stationary flow rate is calculated using the HP law. HP describes a law for the stationary incompressible laminar volumetric flow rate for the flow in a straight pipe. The law connects the flow rate Q to the pressure drop over the length of the pipe Δp through the hydraulic Resistance R_{H}, as seen in Equation (2).

$$Q = \frac{\pi R^4}{8\eta L}\Delta p = \frac{1}{R_{\mathrm{H}}}\Delta p \tag{2}$$

Here, the pipe radius is R, the dynamic fluid viscosity is η, and the pipe length is L. A flow is considered laminar if the dimensionless Reynolds number (Re) is less than 2300. Hereby, the Re number is defined as $\mathrm{Re} = \frac{\rho v D}{\eta}$, with ρ as the density of the fluid, v as the axial fluid velocity, D as the pipe's diameter, and η as the dynamic viscosity.

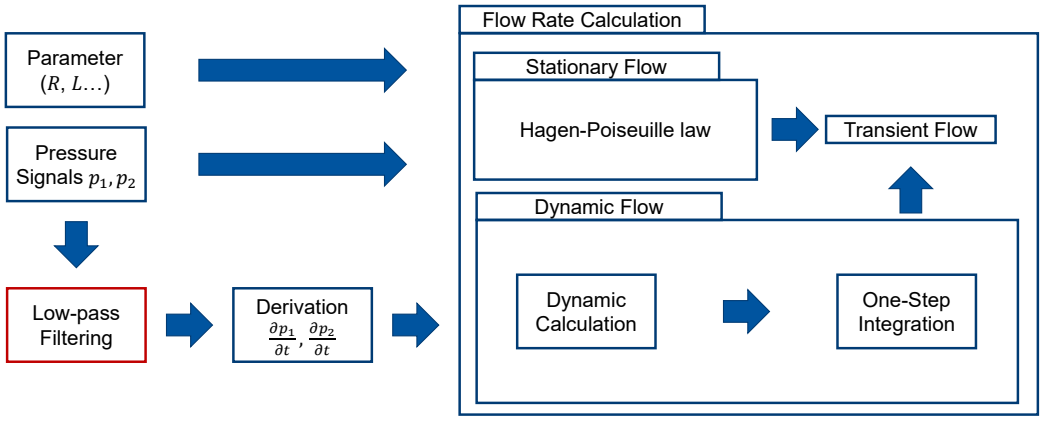

Figure 1. Flowchart for the flow rate calculation using the soft sensor.

In an early work, Brumand-Poor et al. [2] expanded the law of Hagen and Poiseuille to include transient incompressible flow rates. In a subsequent work by Brumand-Poor et al. [3], compressible phenomena were incorporated into the equation for the volumetric flow rate. The resulting equation consists of a stationary part (compare Equation (2)) and a dynamic part, which includes the transient and compressible behavior of the fluid and is presented in Equation (3):

$$Q_2(t_\mathrm{n}) = \frac{1}{R_\mathrm{H}}\Delta p - \frac{1}{R_\mathrm{H}}\left[\int_0^{t_\mathrm{n}} W_{1,\mathrm{dyn}}(t_\mathrm{n}-\tau)\frac{\partial p_1(\tau)}{\partial t_\mathrm{n}}d\tau - \int_0^{t_\mathrm{n}} W_{2,\mathrm{dyn}}(t_\mathrm{n}-\tau)\frac{\partial p_2(\tau)}{\partial t_\mathrm{n}}d\tau\right]. \tag{3}$$

The dynamic part consists of a convolution integral between the dynamic weighting function and the time gradient of the pressure at the pipe's inlet (p_1) and outlet (p_2), respectively. Here, the time is normalized by $t_\mathrm{n} = \frac{\nu}{R^2}t$ so that the time has no dimension and a universal equation can be derived. $\frac{\nu}{R^2}$ represents the time scale of radial diffusion of axial momentum caused by viscous effects. The weighting functions can be split into two parts, one part describing the transient nature of the fluid (W_inc), which is the same for both the inlet and outlet, and one describing the compressible effects at the relative ends of the pipe (W_comp).

$$W_1(t_\mathrm{n}) = W_\mathrm{inc}(t_\mathrm{n}) + W_{1,\mathrm{comp}}(t_\mathrm{n}) \tag{4}$$

$$W_2(t_\mathrm{n}) = W_\mathrm{inc}(t_\mathrm{n}) + W_{2,\mathrm{comp}}(t_\mathrm{n}) \tag{5}$$

A comprehensive derivation and validation with a parameter-distributed simulation of the incompressible and compressible weighting functions are provided in [2] and [3], respectively, and are out of the scope of this paper.

The dynamic weighting functions are then obtained by subtracting the stationary value as follows:

$$W_{1,\mathrm{dyn}}(t_\mathrm{n}) = W_1(t_\mathrm{n}) - 1 \tag{6}$$

$$W_{2,\mathrm{dyn}}(t_\mathrm{n}) = W_1(t_\mathrm{n}) - 1 \tag{7}$$

The convolution integrals in the solution in Equation (3) can be simplified to a one-step integration method, as shown in Brumand-Poor et al. [3], thus simplifying the evaluation of the volumetric flow rate.

$$Q_2(t_\mathrm{n}) = Q_{2,\mathrm{stat}}(t_\mathrm{n}) - [Q_{2,\mathrm{dyn},1}(t_\mathrm{n}) - Q_{2,\mathrm{dyn},2}(t_\mathrm{n})]. \tag{8}$$

$$Q_{2,\mathrm{dyn},1}(t_\mathrm{n}+\Delta t_\mathrm{n}) \approx \frac{1}{R_\mathrm{H}}\sum_{i=1}^{N}\left[Y_{0,i}(t_\mathrm{n})\mathrm{e}^{-n_i\Delta t_\mathrm{n}} + \Delta\dot{p}\frac{m_i}{n_i}(1-\mathrm{e}^{-n_i\Delta t_\mathrm{n}})\right]. \tag{9}$$

$$Q_{2,\mathrm{dyn},2}(t_\mathrm{n}+\Delta t_\mathrm{n}) \approx \frac{1}{R_\mathrm{H}} \sum_{i=1}^{N} \left[Y_{0,i}(t_\mathrm{n}) \mathrm{e}^{-n_i \Delta t_\mathrm{n}} + \Delta \dot{p} \frac{m_i}{n_i} (1 - \mathrm{e}^{-n_i \Delta t_\mathrm{n}}) \right]. \tag{10}$$

Here, $Y_0(t_\mathrm{n})$ is the solution for the dynamic flow rate from the previous timestep. m_i and n_i are the coefficients of the weighting functions in the time domain. $\Delta \dot{p}$ is the pressure difference gradient averaged over the timestep Δt_n.

Further research was conducted regarding the equation for the volumetric flow rate as a soft sensor for real-world applications. In the work by Brumand-Poor et al. [5], the equation was compared to data from a test rig for laminar flows.

The investigations of the soft sensor applied to a real-world test rig showed that filtering is necessary due to signal noise, which does not occur in simulations. That is caused by the fact that the sensor takes the derivative of the pressure signals. By taking the unfiltered derivative, the noise carried by the signal will become amplified, which makes it unusable for calculations. Filtering alters the amplitude and the phase of an investigated signal. Therefore, this work examines whether a basic filter with a small modification of the actual signal is suitable for the soft sensor. Therefore, this work proposes a simple first-order 'Butterworth' filter [22] to pre-process the pressure signals before taking the derivative. This type of filter has a smooth passband without ripples and reduces the signal amplitude with frequencies above a cut-off frequency that the user can set. Therefore, this filter can effectively dampen high-frequency noise. Unlike the Chebyshev filter, which introduces ripples, or the Bessel filter, which has a slow roll-off, the Butterworth filter attenuates noise while preserving signal integrity, ensuring accurate results. Furthermore, only first-order filtering was applied to minimize the effect of altering the amplitude and phase of the signal.

The current work investigates the effect of two different cut-off frequencies on the soft sensor's accuracy. The test cases presented in this work show that a filter with a generic cut-off frequency of 100 Hz, independent from the frequency that should be measured, greatly improves the soft sensor's results. Furthermore, an adequate cut-off frequency is applied to further investigate the filtering effect on accuracy. A filter with 100 Hz has a cut-off frequency so far away from the actual frequency of the investigated pulsations that the phase shift can be neglected for the investigated frequency range.

2.3. Test Rig

The test rig was developed in a prior publication [4] and constructed and utilized to validate the soft sensor in another work [5]. A detailed description of the development and setup is provided in [5].

A dedicated test rig was developed to validate the derived system equations for the soft sensor. Its primary function is to generate a known transient flow rate through a hydraulically smooth, straight pipe that satisfies the assumptions underlying the system equations. The device must also provide pressure measurements at a minimum of two positions along the pipe. These pressure signals are used to calculate the pressure difference required by the system equations. The volumetric flow rate obtained from these calculations is then compared to the flow rate generated by the test rig.

The test rig must provide a range of flow conditions, including laminar and turbulent Reynolds number regimes and stationary and pulsating flows. The most effective method for generating pulsations is to use the motion and geometric displacement of a hydraulic cylinder [4]. The displaced volumetric flow can be approximated by using the kinematics of the cylinder, expressed as $Q_c = Av$. When using this method, it is critical to consider the limitations imposed by compressibility and pressure wave propagation, as neglecting these factors can lead to significant errors in the computation of the flow rate determined by the

cylinder movement. To mitigate errors caused by compressibility effects, it is beneficial to operate at higher pressures as this increases the bulk modulus K and makes it more stable.

Additional errors are introduced by wave reflections within the pipe, which occur when changes in characteristic impedance reflect pressure waves. These impedance changes can result from installations along the pipe or variations in cross-sectional geometry [23]. Therefore, minimizing cross-sectional transitions and terminating the measurement pipe with a low-reflection line terminator (LRLT) is important. An LRLT typically consists of an orifice, a variable cross-section adjustment mechanism, and a downstream volume. By matching the orifice's cross-section to the pipe's characteristic impedance, the LRLT mimics an infinitely long pipe, preventing wave reflections and allowing pressure waves to dissipate in the termination volume. An illustration of the hydraulic circuit of the test rig is provided in Figure 2.

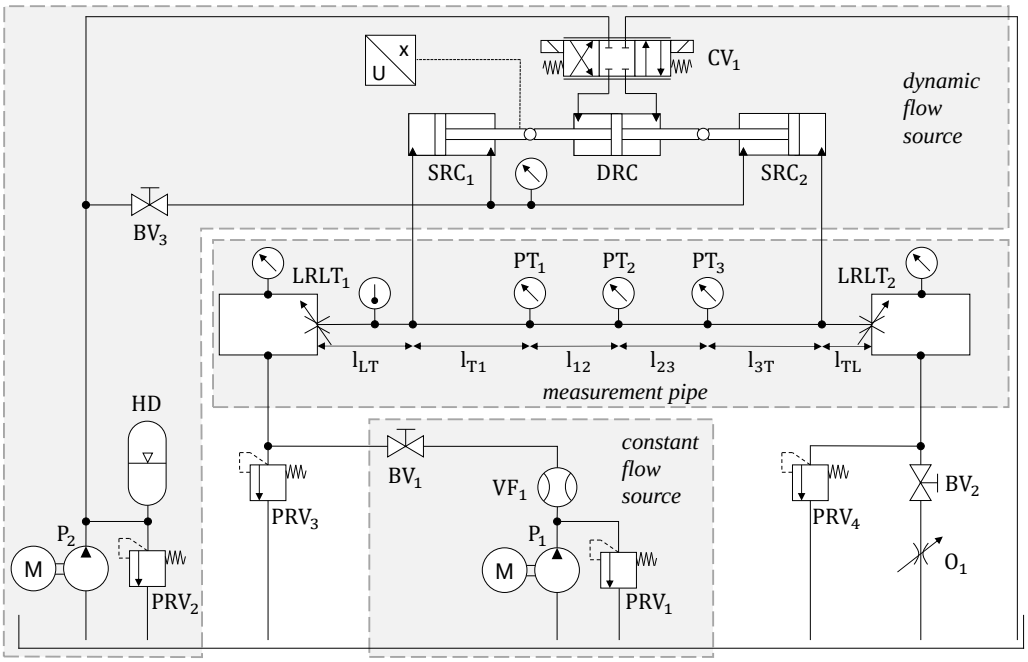

Figure 2. The hydraulic circuit of the test rig [5].

The main feature of the test rig is a measuring pipe with a length of 3.22 m with three designated points for pressure monitoring. The distances between the pressure transducers PT_1 and PT_2 and between PT_2 and PT_3 are $l_{12} = 0.33$ m and $l_{23} = 0.47$ m, respectively. To mitigate pressure wave reflections, the measuring pipe is equipped with $LRLT_{1,2}$ at both ends. Each LRLT is located $l_{LT} = l_{TL} = 0.36$ m from the nearest T-junction. In addition, an adjustable orifice, O_1, is used to regulate the pressure within the pipe to minimize compressibility effects.

The steady flow system connected to $LRLT_1$ includes a hydraulic pump (P_1), a pressure relief valve (PRV_1), and a volumetric flow sensor (VF_1). On the other side, the dynamic flow source integrates a double-rod cylinder (DRC) that drives two single-rod cylinders ($SRC_{1,2}$), generating fluctuating volumetric flows. The T-joints connecting the measurement pipe to the dynamic flow source are positioned $l_{T1} = 1.5$ m from PT_1 and $l_{3T} = 0.2$ m from PT_3, providing sufficient inlet and outlet zones.

The double-rod cylinder is controlled by a servo valve CV_1, which adjusts the amplitude and waveform of the flow, allowing a range of operating scenarios. Piston velocity is tracked by a position sensor mounted on one of the rods. The dynamic flow system also includes a second hydraulic pump (P_2), a pressure relief valve (PRV_4), and a set of

switching valves (SV_3). The switching valves are configured to pre-pressurize the single-rod cylinders, thereby balancing the forces exerted by the pressure within the sensing pipe and reducing the mechanical stress on the connections. The coupling mechanism between the single-rod cylinders ensures a constant volume of fluid in the pipe as the suction of one cylinder compensates for the displacement of the other.

Adjustments to the LRLT orifices are based on the average volumetric flow, Q_m, provided by the pump P_1, as defined in Equation (11). Deviations of the flow rate through the orifice from Q_m change the characteristic impedance and introduce errors in estimating the flow rate, especially at higher frequencies [4]. Switching valves $SV_{1,2}$ allow the device to operate in an oscillating or pulsating mode, where the pulsating mode superimposes the mean flow rate, Q_m, with the dynamic component, $Q_c = A \cdot v$. The volumetric flow rate derived from the pressure measurements is compared to the experimental flow rate calculated as $Q = Q_m + Q_c$ to validate the soft sensor.

$$\Delta p = \frac{Q_m \cdot \rho \cdot a}{2 \cdot A_{pipe}} \tag{11}$$

Figure 3 illustrates the implementation of the test rig design. The following key elements are highlighted in the figure: The $LRLT_{1,2}$, marked with red circles, are positioned at both ends of the measuring pipe (outlined in orange). The coupled cylinders, outlined in blue, are key in generating the dynamic flow rate by driving the oscillatory fluid motion.

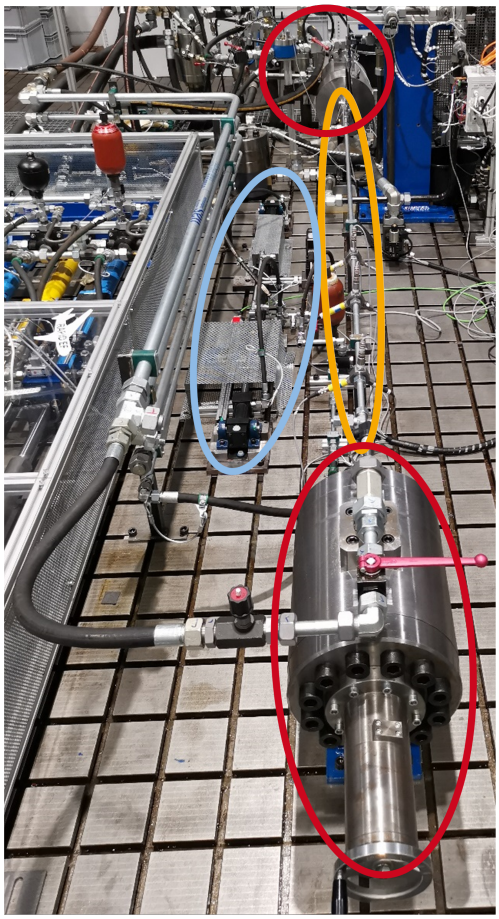

Figure 3. Picture of the constructed test rig [5].

2.4. Test Cases

The first three test cases consider the sinusoidal flow pulsations with frequencies of 5, 10, and 15 Hz, respectively. These tests were conducted under laminar flow conditions (Re $<$ 2300) for which the soft sensor has been previously validated [3]. This work investigates the impact of filtering the pressure transducer signals. All tests were carried out with a system pressure of 100 bar to minimize the compression effect for calculating the reference flow rate.

The last two test cases are pulsations with a frequency of 5 Hz. The difference from the first three test cases lies in the Reynolds number, which was chosen to be higher than the threshold of laminar flow. Therefore, the flow in these test cases was non-laminar. The investigated Reynolds numbers are higher than 2300 and less than 4000, which means that the flow is in the transitional regime. These test cases show the potential of the soft sensor in regions outside the laminar flow and thus broaden the validity range of the soft sensor. The five test cases are defined in Table 1.

Table 1. Parameters for each test case (The fluid model determining the viscosity and density is presented in Appendix A).

Test Case	Mean Volumetric Flow Rate Q_{Stat} [L/min]	Reynolds Number Re [-]	Frequency f [Hz]	Temperature T [°C]	Kinematic Viscosity ν [mm^2/s]	Density ρ [kg/m^3]
Sine (Figures 4–8)	50	1339	5	35.8	58.1	863.2
Sine (Figures 9 and 10)	50	1355	10	36.2	57	863
Sine (Figures 11 and 12)	50	1355	15	36.2	57	863
Sine (Figures 13 and 14)	77	3279	5	47	35.8	855.7
Sine (Figures 16 and 17)	86	2703	5	39.9	48.3	860.5

A first-order low-pass filter with varying cut-off frequencies filtered each test case. For the laminar 5 Hz oscillation and the two turbulent test cases, the unfiltered data are shown, as well as the filtered data with cut-off frequencies of 100 Hz and one that is 1 Hz above the expected frequency. For example, for the case of the 10 Hz oscillation, the cut-off frequency of the low-pass filter was set to 11 Hz.

3. Results

3.1. Laminar Test Cases

Five test cases, three laminar and two non-laminar flows, were investigated. For each test, the calculated flow rate from the pressure transducers ("Soft Sensor") is compared to the measured signal from the test rig ("Test Rig"). For the case of laminar flow with a pressure oscillation of 5 Hz, the results are shown in the following three Figures 4–8. The three figures compare the different filtering corner frequencies of the soft sensor to the measured flow rate. Figure 4 shows the unfiltered result of the soft sensor in comparison to the test rig. The effect of taking the derivative of the pressure signals during the calculation of the soft sensor can be seen in the deviation from the test rig flow rate.

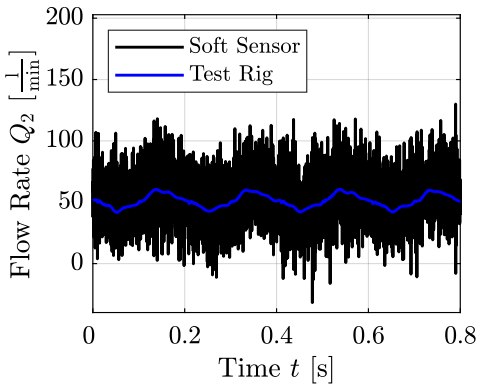

Figure 4. Unfiltered flow rate compared to the test rig for a laminar 5 Hz pulsation.

The corresponding pressure difference, as well as the gradient of the difference, that was used to calculate the unfiltered flow rate from Figure 4 can be seen in Figure 5 and Figure 6, respectively. It can be observed that the periodicity of the signal is partly visible in the pressure difference but is completely unrecognizable in the gradient.

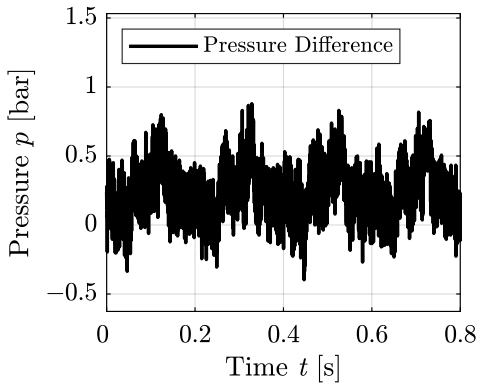

Figure 5. Unfiltered pressure difference for 5 Hz.

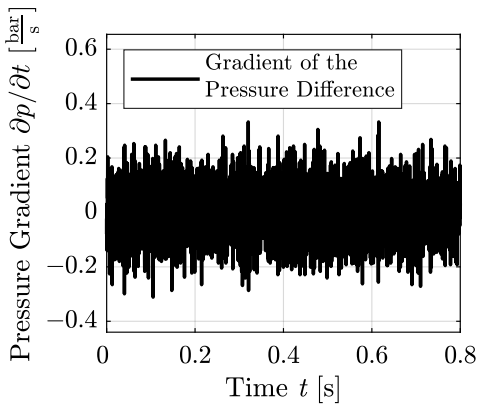

Figure 6. Unfiltered gradient of the pressure difference for 5 Hz.

This behavior is improved in Figures 7 and 8. Interestingly, a low-pass filter with a corner frequency of 100 Hz, as shown in Figure 7, dramatically improves the soft sensor's result. Interestingly, the flow rate computed by the test rig resembles each other for the unfiltered and filtered case. The best result is obtained using a low-pass filter with a corner frequency of 6 Hz (1 Hz above the expected frequency), as seen in Figure 8.

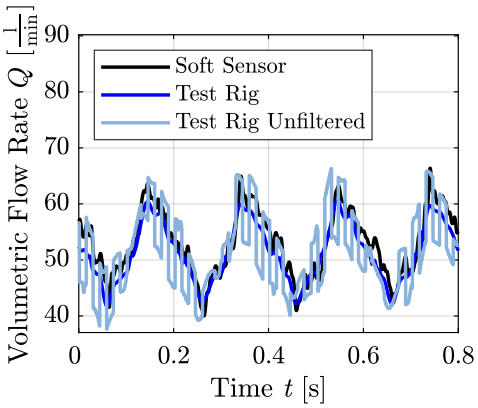

Figure 7. Filtered flow rate (100 Hz cut-off).

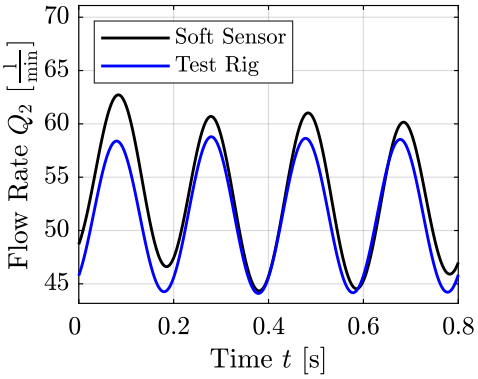

Figure 8. Filtered flow rate (6 Hz cut-off).

The next test case was a laminar flow with a pressure oscillation of 10 Hz. This time, presenting the unfiltered results is omitted due to redundancy to the first test case. Figures 9 and 10 show that a 100 Hz low-pass filter yields accurate results, which can be further improved using a 11 Hz low-pass filter.

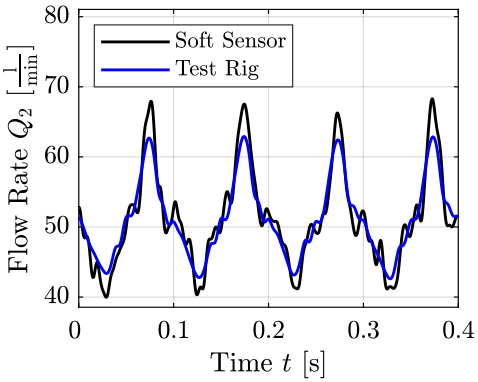

Figure 9. Filtered flow rate (100 Hz cut-off).

The third test case presented in this work is laminar flow with 15 Hz pressure oscillations. For this case, Figure 11 shows the filtering of the pressure signals with a 100 Hz low-pass filter, and Figure 12 shows filtering using a 16 Hz low-pass filter. Using the filter with a cut-off frequency closer to the expected frequency improved the result from the soft sensor. To sum up, the effect of basic filtering for the soft sensor can be observed for all three laminar test cases. Even filtering with 100 Hz improves the results greatly.

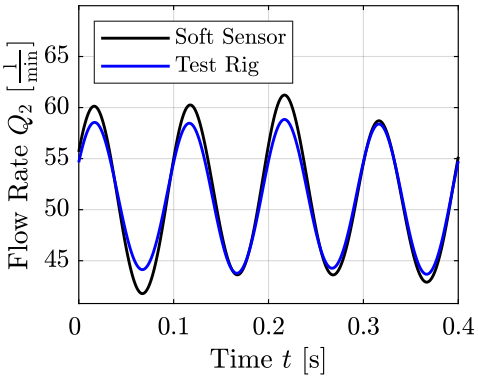

Figure 10. Filtered flow rate (11 Hz cut-off).

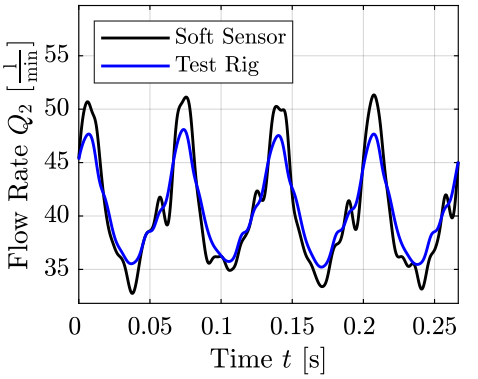

Figure 11. Filtered flow rate (100 Hz cut-off).

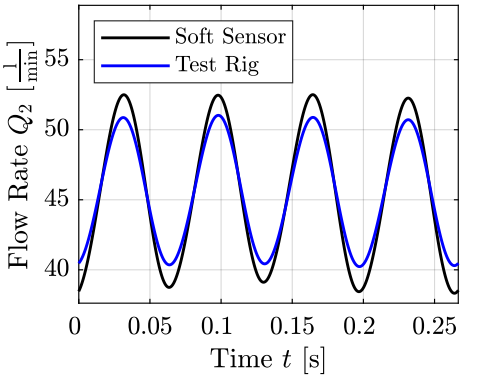

Figure 12. Filtered flow rate (16 Hz cut-off).

3.2. Non-Laminar Test Cases

The following two test cases are pulsation with a frequency of 5 Hz. Compared to the previously presented results, the flows are non-laminar due to their high Reynolds number, Re = 3279 and 2703, respectively. These test cases are utilized to investigate the accuracy of the soft sensor for non-laminar flow and the impact of filtering on the measuring method. In Figure 13, the unfiltered volumetric flow rate of the soft sensor is shown.

Like the laminar test cases, the flow rates do not match due to the high level of noise in the pressure derivatives. Compared to this result, applying a 100 Hz filter, as shown in Figure 14, improves the results, and using a 6 Hz first-order Butterworth filter improves the results dramatically as shown in Figure 15.

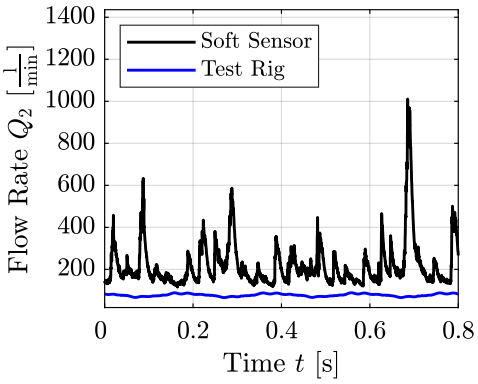

Figure 13. Unfiltered flow rate compared to the test rig for a non-laminar 5 Hz pulsation.

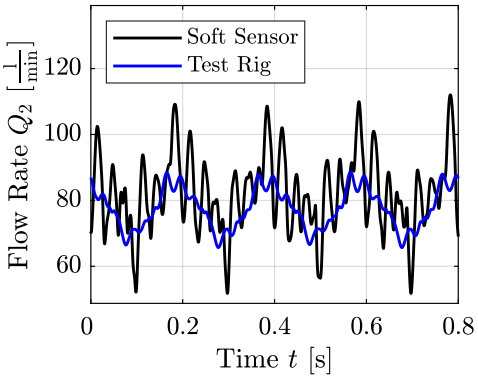

Figure 14. Filtered flow rate (100 Hz cut-off).

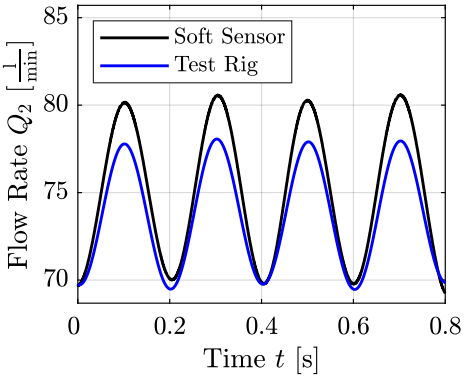

Figure 15. Filtered flow rate (6 Hz cut-off).

In contrast to the laminar test cases, a 100 Butterwort filter increases the accuracy, but suitable results are obtained by applying a filter with a cut-off frequency of 6 Hz. This finding is underlined in Figures 16 and 17, where a 100 Hzfilter does not suffice to match the test rig and soft sensor. However, suitable filtering with 6 Hz matches the test rig and soft sensor, as shown in Figure 17. For both test cases, the soft sensor can compute the transient volumetric flow rate accurately with a basic first-order Butterworth filter, demonstrating the soft sensor's wide range of validity.

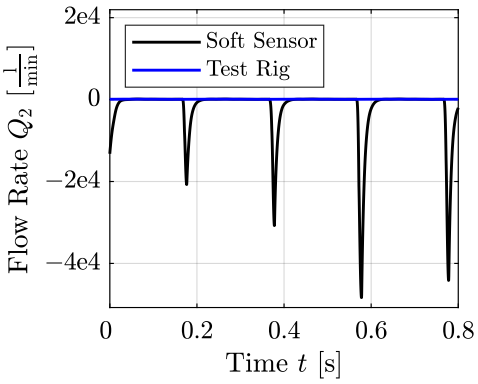

Figure 16. Filtered flow rate (100 Hz cut-off).

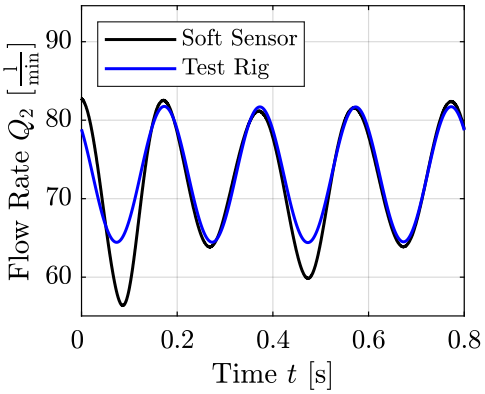

Figure 17. Filtered flow rate (6 Hz cut-off).

4. Discussion

This paper presents an innovative approach to transient flow measurement. It starts by reviewing the methods and transient models. Then, it describes the analytical soft sensor, the experimental test rig, and the validation process using various test cases. The sensor provides accurate, real-time flow rate calculations, even under challenging conditions with basic filtering of the pressure signals. This underlines the robustness of the soft sensor since no sophisticated filtering algorithm is required for accurate volumetric flow rate determination. Furthermore, the paper demonstrates that the soft sensor's range of validity extends beyond the laminar regime by showing its high accuracy for non-laminar transient flow.

The results indicate that basic filtering is essential for achieving reasonable measurement accuracy. Without filtering, unfiltered pressure signals as input to the soft sensor proved ineffective for both laminar and non-laminar flows. This is mainly due to the derivation of the pressure signals, which is utilized to compute the dynamic volumetric flow rate and is especially prone to error due to signal noise. In the laminar flow test cases, a simple 100 Hz filter significantly improved the accuracy of the measurements, bringing the results within an acceptable range. A 100 Hz filter also demonstrated its benefit for non-laminar flows, though further refinement is necessary to achieve optimal results. The pressure transducers have a lower accuracy than the position sensor, which is utilized to obtain the reference volumetric flow rate. More precisely, the pressure transducers have a full-scale error of 0.25%. Related to their range of 200 bar yields an absolute error of 0.5 bar for each sensor. The motion sensor has an absolute error of 0.5 µm. As shown in Figure 5, the pressure difference in the measurements peaks at 0.8 bar. In the worst case, both transducers producing their maximum error would result in a total error of 1 bar, which is above the maximum measured difference. Furthermore, the dynamic flow rate is

computed based on the gradient of the pressure difference, which exhibits strongly noisy behavior, as shown in Figure 6. These two plots underline the importance of filtering the signal to achieve high accuracy for the soft sensor. Regarding the flow rate computed by the test rig, as discussed above, the sensor exhibits much higher accuracy, reducing the need for filtering the signals. This can be seen in Figure 8, where the unfiltered volumetric flow rate is the product of velocity, and the cylinder area strongly resembles the filtered test right flow rate.

In the validation, the investigated frequencies were known beforehand. However, in many applications, like control, the frequency range is also known, which allows for the direct utilization of adequate filtering for the soft sensor. For applications where the frequencies might not be known, basic filtering of 100 Hz can dramatically increase the accuracy in most cases. Furthermore, for a more advanced approach, established methods such as the Fast Fourier Transform (FFT) can identify pulsation frequencies, enabling targeted filtering during operation. Therefore, no complicated pre-processing is necessary, underlining the robustness and easy-to-use nature of the soft sensor. Machine learning models, particularly adaptive filtering techniques or neural network-based denoising approaches, could refine signal quality by learning from system behavior in real time. Such methods could enhance high-frequency noise accuracy further by dynamically adapting to varying signal conditions.

The precision of the pressure sensor is a key factor in the soft sensor's performance. The soft sensor's design benefits from a minimal distance between the two pressure transducers, which results in only a slight pressure drop, especially in laminar flow conditions, which are the most common in fluid power applications. Since these slight pressure differences often fall within the sensors' measurement resolution, measurement reliability may be affected. This issue can be alleviated through sensor calibration and simple filtering techniques, as illustrated in this work. The noise level in the pressure measurements defines the minimum measurable volumetric flow rate, as the analytical model does not impose a theoretical lower limit. Dominant noise sources include mechanical vibrations, electromagnetic interference, and sensor resolution limits, all of which can introduce fluctuations that disrupt small pressure differences. The flow regime defines the upper limit. The analytical model assumes a laminar flow. However, our findings also underline the potential to successfully apply the soft sensor to transitional flow regimes. The upper limit for the analytical model is most likely following a turbulent flow regime. However, this area is usually not operated in fluid power applications due to the additional friction losses caused by the turbulent nature of the pipe flow. If applications with turbulent flow are of interest in future works, transient, turbulent friction models from Vardy et al. can be integrated into the analytical soft sensor [24]. Additionally, the soft sensor relies on an accurate fluid model to function effectively. Changes in fluid properties, such as variations in kinematic viscosity and density due to fluctuations in pressure and temperature, must be well understood. If these variations are not adequately accounted for, significant errors can occur. While established fluid models can be employed and parameterized experimentally, their precise implementation is crucial for maintaining measurement accuracy. Another critical factor is the proper installation of the pressure sensors. External disturbances, such as mechanical vibrations, can introduce measurement errors. Even minor external influences can compromise accuracy due to the recorded pressure differences. Ensuring stable sensor mounting and isolating the setup from mechanical disruptions are essential in improving measurement reliability. Another challenge associated with the soft sensor is the insufficient inlet and outlet pipe lengths needed to achieve fully developed flow conditions. In laminar flow regimes, a standard in fluid power systems, the required pipe length increases proportionally with the Reynolds number. If the inlet section is too short,

substantial measurement errors can arise. To mitigate this, future research will explore integrating inlet flow models to reduce the dependency on extended pipe sections. Careful system design, sensor calibration, and refined modeling techniques can address the soft sensor's limitations. With these improvements, the soft sensor can become a widely adopted solution in industrial applications.

5. Conclusions

This work illustrates the ability of our soft sensor to accurately capture transient flows with a first-order low-pass filter. Furthermore, the analytical soft sensor can capture transitional flows, which exhibit a higher Reynolds number than laminar flows. The paper introduces the currently available flow models and volumetric flow rate measurement techniques. Subsequently, it briefly presents the soft sensor. Afterward, the soft sensor-constructed test rig and the examined test cases are discussed. The soft sensor accurately determines flow rates for Reynolds numbers up to 3279 with a pulsating flow of 10 Hz and laminar flows with a pulsation of up to 15 Hz.

The findings demonstrate that the sensor effectively covers a broad range of Reynolds numbers, making it highly suitable for several fluid power applications. The results achieved in this initial study for non-laminar flows show promising accuracy. However, further investigation is essential, as the non-laminar regime includes transitional and turbulent flows. These flow types are notoriously challenging to describe, particularly when modeled physically. Consequently, mathematical models used in these scenarios are often either computationally intensive or inaccurate due to simplifications made. This underscores the importance of advancing the soft sensor's capabilities to address these complexities, ensuring its applicability to a broader range of fluid dynamics applications. Notably, most fluid power systems aim to operate in a laminar flow regime due to the increased power loss based on friction, which increases for non-laminar flows.

The results further demonstrate the sensor's potential for a wide range of industrial applications, particularly in real-time condition monitoring and control, where precise measurements are critical. The sensor facilitates hydraulic power computation by monitoring pressure and flow rates, contributing valuable insights for predictive maintenance. Unlike traditional numerical methods, which often face a trade-off between real-time processing and high accuracy, the soft sensor delivers both, providing a robust and efficient solution for demanding operational environments. In addition to general monitoring, the soft sensor can be applied to pump performance analysis under varying conditions, ensuring optimal operation even at high frequencies. Based on an analytical model, its real-time flow rate measurements improve precision in applications like cylinder control and press operations, where quick, accurate flow calculations are crucial. Furthermore, its ability to track flow rates aids in performance evaluation and anomaly detection, enabling proactive maintenance strategies to minimize downtime and reduce operational costs. These results represent a significant advancement in soft sensor methods for transient volumetric flow rate determination and suggest that an application on a large-scale industrial system can yield good results. This is further underlined by the wide range of validity regarding the Reynolds number of the analytical soft sensor. Bigger pipe diameters result in a higher Reynolds number. However, most industrial applications aim to stay within the laminar regime or avoid the turbulent flow regime. Thus, no additional friction loss is introduced to the system. The soft sensor can measure laminar and transitional flows, thus suggesting its promising application in large-scale systems. Furthermore, the soft sensor can be integrated into a fluid model, which allows it to be applied to a wider range of systems. Future research will focus on higher-frequency flows, a topic previously explored in earlier

work [2,3]. The impact of reflections, compressibility, and varying pressure profiles will also be examined.

Author Contributions: Conceptualization, F.B.-P., T.K., A.H., C.R. and K.S.; Data curation, F.B.-P., T.K. and M.H.; Formal analysis, F.B.-P., T.K., A.H. and C.R.; Funding acquisition, F.B.-P. and K.S.; Investigation, F.B.-P. and A.H.; Methodology, F.B.-P., T.K. and A.H.; Project administration, F.B.-P. and A.H.; Resources, F.B.-P., T.K., A.H. and K.S.; Software, F.B.-P., T.K., A.H. and C.R.; Supervision, F.B.-P. and K.S.; Validation, F.B.-P., T.K. and A.H.; Visualization, F.B.-P., T.K. and A.H.; Writing—original draft, F.B.-P. and T.K.; Writing—review and editing, F.B.-P., T.K., M.H. and K.S. All authors have read and agreed to the published version of the manuscript.

Funding: The IGF research project 21475 N/1 of the research association Forschungskuratorium Maschinenbau e. V. (FKM), Lyoner Straße 18, 60528 Frankfurt am Main was supported by the budget of the Federal Ministry of Economic Affairs and Climate Action through the AiF, within the scope of a program to support industrial community research and development (IGF) based on a decision of the German Bundestag.

Institutional Review Board Statement: Not applicable.

Informed Consent Statement: Not applicable.

Data Availability Statement: The datasets presented in this article are not readily available because the data are part of an ongoing study.

Conflicts of Interest: The authors declare no conflicts of interest.

Abbreviations

The following abbreviations are used in this manuscript:

BV	Ball Valve
CV	Control Valve
DRC	Double-rod Cylinder
FFT	Fast Fourier Transform
HD	Hydraulic Damper
HP	Hagen–Poiseuille
LRLT	Low-reflection line terminator
O	Adjustable Orifice
P	Hydraulic Pump
PIV	Particle Image Velocimetry
PT	Pressure Transducer
Re	Reynolds number
SRC	Single-rod Cylinder
SV	Switching Valve
VF	Volumetric Flow Rate Sensor

Nomenclature

Symbol	Definition	Unit
*	Denotation of a Variable in the Laplace Domain	$[m^2/s]$
A	Cross-section of the Cylinder	$[m^2]$
A_1	First Parameter of Temperature-dependent Viscosity Model	$[m^2/s]$
A_2	First Parameter of the Temperature-dependent Density Model	$[kg/^\circ C\ m^3]$
A_D	Geometric Parameter	$[m^2]$
A_{pipe}	Cross-section of the Pipe	$[m^2]$
B_1	Second Parameter of the Temperature-dependent Viscosity Model	$[-]$
B_2	Second Parameter of the Temperature-dependent Density Model	$[kg/m^3]$
C	Third Parameter of Temperature-dependent Viscosity Model	$[1/^\circ C]$
Dn	Dissipation Number	[-]

f	Frequency	[Hz]
K	Bulk Modulus	[Pa]
l	Pipe section length	[m]
L	Length of the Pipe	[m]
Δp	Pressure Difference	[-]
p_1	Pressure at Inlet	[bar]
p_2	Pressure at Outlet	[bar]
Q	Volumetric Flow Rate	[m^3/s]
Q_c	Volumetric Flow Rate from the Cylinder	[m^3/s]
Q_m	Mean Volumetric Flow Rate	[m^3/s]
Q_{Stat}	Stationary Volumetric Flow Rate	[m^3/s]
Q_{dyn}	Dynamic Volumetric Flow Rate	[m^3/s]
Q_i	Volumetric flow rate at Inlet: $i = 1$ and Outlet: $i = 2$	[m^3/s]
R	Radius of the Pipe	[m]
Re	Reynolds Number	[-]
R_H	Hydraulic Resistance	[$Pa/(m^3/s)$]
t	Time	[s]
t_n	Normalized Time	[-]
v	Axial Fluid Velocity	[m/s]
v	Velocity of the Cylinder	[m/s]
W_i	Weighting function at End $i \in \{1,2\}$ of the Pipe	[-]
$W_\mathrm{i}^{'}$	Weighting function at port $i \in \{1,2\}$	[-]
$W_\mathrm{i,dyn}$	Negative of $W_\mathrm{i,dyn}^{'}$	[-]
$W_\mathrm{1,comp}$	Compressible Weighting Function at port 1	[-]
W_inc	Incompressible Weighting Function	[-]
α_D	Discharge Coefficient	[-]
η	Dynamic Viscosity	[Pas]
ν	Kinematic Viscosity	[m^2/s]
ρ	Fluid Density	[kg/m^3]
τ	Time	[s]
τ_n	Normalized Time	[s]

Appendix A. Fluid Model

The fluid model is a critical aspect of the analytical soft sensor. It is primarily described by the density *rho* and the kinematic viscosity *nu*. To ensure the accurate determination of these values, a temperature-dependent model was created by adequately measuring *rho* and *nu* over a temperature span [25]. The following models were fitted by experimental data:

$$\nu = A_1 \cdot exp(B_1/(C+T)) \tag{A1}$$

$$\rho = A_2 \cdot T + B_2 \tag{A2}$$

with A_1, B_1, C, A_2, B_2 being the curve-fitted parameters, which are stated in Table A1 with the coefficient of determination R^2 and the adjusted value $R^2_{adj.}$ for both equations.

Table A1. Parameters for the fluid model.

Parameter	A_1	B_1	C	A_2	B_2	R^2	$R^2_{adj.}$
ν	0.11	837.5	97.73	–	–	0.9999	0.9999
ρ	–	–	–	−0.6064	882.33	1	1

References

1. Richardson, E.G.; Tyler, E. The transverse velocity gradient near the mouths of pipes in which an alternating or continuous flow of air is established. *Proc. Phys. Soc.* **1929**, *42*, 1–15. [CrossRef]
2. Brumand-Poor, F.; Kotte, T.; Pasquini, E.; Kratschun, F.; Enking, J.; Schmitz, K. Unsteady flow rate in transient, incompressible pipe flow. *Z. Angew Math Mech.* **2024**, *105*, e202300125. [CrossRef]
3. Brumand-Poor, F.; Kotte, T.; Pasquini, E.; Schmitz, K. Signal Processing for High-Frequency Flow Rate Determination: An Analytical Soft Sensor Using Two Pressure Signals. *Preprints* **2024**. [CrossRef]
4. Brumand-Poor, F.; Schüpfer, M.; Merkel, A.; Schmitz, K. Development of a Hydraulic Test Rig for a Virtual Flow Sensor. In Proceedings of the Eighteenth Scandinavian International Conference on Fluid Power (SICFP'23), Tampere, Finland, 30 May–1 June 2023.
5. Brumand-Poor, F.; Kotte, T.; Schüpfer, M.; Figge, F.; Schmitz, K. High-Frequency Flow Rate Determination—A Pressure-Based Measurement Approach. *Preprints* **2024**. [CrossRef]
6. Manhartsgruber, B. Instantaneous Liquid Flow Rate Measurement Utilizing the Dynamics of Laminar Pipe Flow. *J. Fluids Eng.* **2008**, *130*, 121402. [CrossRef]
7. Kashima, A.; Lee, P.; Ghidaoui, M. A selective literature review of methods for measuring the flow rate in pipe transient flows. In Proceedings of the BHR Group—11th International Conferences on Pressure Surges, Lisbon, Portugal, 24–26 October 2012; pp. 733–742.
8. Wiklund, D.; Peluso, M. Quantifying and Specifying the Dynamic Response of Flowmeters. *Conf. ISA* **2002**, *422*, 463–476.
9. Brunone, B.; Berni, A. Wall Shear Stress in Transient Turbulent Pipe Flow by Local Velocity Measurement. *J. Hydraul. Eng.* **2010**, *136*, 10. [CrossRef]
10. Grant, I. Particle image velocimetry: A review. *Proc. Inst. Mech. Eng. Part C J. Mech. Eng. Sci.* **1997**, *211*, 55–76. [CrossRef]
11. Brereton, G.J.; Schock, H.J.; Rahi, M.A.A. An indirect pressure-gradient technique for measuring instantaneous flow rates in unsteady duct flows. *Exp. Fluids* **2006**, *40*, 238–244. [CrossRef]
12. Brereton, G.J.; Schock, H.J.; Bedford, J.C. An indirect technique for determining instantaneous flow rate from centerline velocity in unsteady duct flows. *Flow Meas. Instrum.* **2008**, *19*, 9–15. [CrossRef]
13. Sundstrom, L.R.J.; Saemi, S.; Raisee, M.; Cervantes, M.J. Improved frictional modeling for the pressure-time method. *Flow Meas. Instrum.* **2019**, *69*, 101604. [CrossRef]
14. Foucault, E.; Szeger, P. Unsteady flowmeter. *Flow Meas. Instrum.* **2019**, *69*, 101607. [CrossRef]
15. García García, F.J.; Fariñas Alvariño, P. On the analytic explanation of experiments where turbulence vanishes in pipe flow. *J. Fluid Mech.* **2022**, *951*, A4. [CrossRef]
16. García García, F.J.; Fariñas Alvariño, P. On an analytic solution for general unsteady/transient turbulent pipe flow and starting turbulent flow. *Eur. J. Mech.-B/Fluids* **2019**, *74*, 200–210. [CrossRef]
17. Urbanowicz, K.; Bergant, A.; Stosiak, M.; Deptuła, A.; Karpenko, M. Navier–Stokes Solutions for Accelerating Pipe Flow—A Review of Analytical Models. *Energies* **2023**, *16*, 1407. [CrossRef]
18. Urbanowicz, K.; Bergant, A.; Stosiak, M.; Karpenko, M.; Bogdevičius, M. Developments in analytical wall shear stress modelling for water hammer phenomena. *J. Sound Vib.* **2023**, *562*, 117848. [CrossRef]
19. Bayle, A.; Rein, F.; Plouraboué, F. Frequency varying rheology-based fluid–structure-interactions waves in liquid-filled visco-elastic pipes. *J. Sound Vib.* **2023**, *562*, 117824. [CrossRef]
20. Bayle, A.; Plouraboue, F. Laplace-Domain Fluid–Structure Interaction Solutions for Water Hammer Waves in a Pipe. *J. Hydraul. Eng.* **2024**, *150*, 2. [CrossRef]
21. Hucko, S.; Krampe, H.; Schmitz, K. Evaluation of a Soft Sensor Concept for Indirect Flow Rate Estimation in Solenoid-Operated Spool Valves. *Actuators* **2023**, *12*, 148. [CrossRef]
22. Butterworth, S. On the Theory of Filter Amplifiers. *Exp. Wirel. Wirel. Eng.* **1930**, *7*, 536–541.
23. Schmitz, K.; Murrenhoff, H. *Hydraulik*, vollständig neu bearbeitete auflage ed.; Reihe Fluidtechnik; Shaker Verlag: Aachen, Germany, 2018; Volume 2.
24. Vardy, A.E.; Brown, J.M. Transient Turbulent Friction In Smooth Pipe Flows. *J. Sound Vib.* **2003**, *259*, 1011–1036. [CrossRef]
25. Bartel, D. *Simulation von Tribosystemen*; Springer: Berlin/Heidelberg, Germany, 2010. [CrossRef]